Heat and mass transfer Analysis of Radiation and MHD buoyancy-driven mixed convection slips flow over an inclined plate with thermophoresis effects

M. Sreedhar Babu[1], P. Naga Raju[2], B. Mallikarjuna Reddy[3]
[1,2,3]Department of Applied Mathematics, Yogi Vemana University, Kadapa, Andhra Pradesh, India.
* Corresponding author E-mail: chinna20021996@gmail.com

Article History: Received: 24-01-2023 **Revised:** 05-03-2023 **Accepted:** 25-05-2023

ABSTRACT: This inquiry examines the steady-state thermal radiation and MHD buoyancy-driven mixed convection slips flow over a porous inclined plate. Using the similarity technique, PDEs are transformed into nonlinear ODEs. Using Maple software, the Runge-Kutta fourth-order method is used to numerically solve these equations. The impacts of different effects of the magnetic field, porosity, buoyancy force parameter, velocity, temperature, concentration slips, thermal radiation, thermophoresis, and Schmidt number parameters on temperature, velocity, and concentration profiles have been examined. Nusselt number, Skin friction Sherwood no are also included. The computed results are shown graphically and in a table. While the porosity and magnetic field parameters are increasing, the velocity profile is decreasing on inclined plates. The temperature rises as the parameters measuring radiation and magnetic field reach larger values. As the Sherwood number and Nusselt number across an inclined plate increase, the impression of Eckert number, thermal radiation, and magnetic field values seems to be growing. It has many applications, such as including die-extruded polymer sheets, continuous casting, and biomedical.

KEYWORDS: MHD, Joule heating, linear thermal radiation, pours medium, thermophoresis.

1. Introduction

The main objective of boundary layer analysis is to properly forecast the intricate flow characteristics near the boundary layer. Many scientists studying boundary layers and thermal conduction have thought of examining this phenomenon. Various studies have suggested using either a horizontal or an inclined flat plate, while others have suggested using a vertical plate. There are several important industrial uses for the study of boundary layers and heat and mass transmission, aerodynamic extrusion of plastic sheets, including die-extruded polymer sheets, continuous casting, glass-blowing-spun fibres, etc. Badruddin et al. [1] examined the influence of thermal radiation and porous medium on a vertical plate. Khan et al. [2] explored MHD micropolar fluids hybrid nanofluids over a vertical plate. The impact of dusty slip flows through an SCNT-

MCNT over an endlessly inclined plate was studied by [3]. several researchers addressed the inclined and flat plates[4–6].

Researchers have paid close attention to the problems of magnetohydrodynamic (MHD) natural convective flow in many fields of technology and science, the nuclear engineering. industrial power engineering, plasma jet engines, accelerators, generators, industrial processes in material processing and metallurgy including pumps. The heat transportation of an MHD hybrid nanofluid flow across a stretched sheet is studied by Raghunath [7]. Sudarsana Reddy et al [8] investigate the influence of magnetic fields, and heat generation on the flow of a nanofluid across an inclined plate with a porous medium. Goyal et al.[9] examined the MHD flow of a nanofluid over an inclined plate. Mustafa [10] discussed the Buongiorno model, MHD nanofluid flow along a converging or diverging channel. several researchers addressed the MHD.[11–16].

Thermal radiation explains the characteristics of the electromagnetic energy emitted by a material as a function of its heat, and these characteristics are influenced by temperature. Thermal radiation causes heat to be emitted by increasing thermal diffusivity. Thermal radiation is often employed in commercial and high-temperature uses, solar panels, and nuclear power plants, including electricity, food, missiles, gas turbines, aerospace engineering, and drug delivery. The influence of radiation and MHD on blood as a base fluid and gold as nanofluids over a curved surface were discussed by Khan *et al*.[17]. Shafiq et al. [18] examined the influence of thermal radiation and MHD micropolar fluid flow on the inclined sheet. Gulle et al. [19] discussed the effects of thermal radiation and MHD Jeffrey fluid flow on the inclined porous plate. Maghsoudi et al. [20] investigated the effect non-Newtonian fluid of thermal radiation flow through an infinity of vertical flat plates.[21–25]

The presence of a porous substance or material is porous. biological tissues, Rocks, the ground, sand, and wooden structures all have porous media since they are made of natural materials. The porosity of this material is often used for modifications, such as some applications of porous media have numerous applications in thermal insulation, including geothermal systems, such as tissue replacement and biomedical applications and engineering which has piqued the interest of researchers and scholars to conduct more research. Barik et al. [26] studied the MHD flows of a Hybrid nanofluid over a porous Plate. Hydromagnetic free convection flow via an infinite vertical plate in a porous media is studied by Bang Sarma et al. [27]. Many researchers are discussed by Puros Medium.[25,28,29].

This study of heat transfer and mass transfer analysis of MHD buoyancy-driven mixed convection slips flow over a porous inclined plate with thermophoresis. so, all parameters are taken into consideration. We employed water as the basis fluid in this model, and coupled nonlinear PDEs into ODEs by using self-similarity are used to solve the Numerical Method (RK 4 th order Method) in Maple software. The impacts of so many effects of the porosity, magnetic field, buoyancy parameter, slips conditions parameters, thermal radiation, Schmidt number, and thermophoresis parameters on temperature, velocity, and concentration profiles have been examined. Nusselt number, Skin friction Sherwood no are also included. The computed results are shown graphically and in a table. It has many applications, such as including die-extruded polymer sheets, glass-blowing-spun fibres, continuous casting, and biomedical uses in antimicrobial agents, diagnostic, and drug delivery.

2. Formulation in mathematics

Consider a incompressible, steady, 2D modal, and Magnetohydrodynamic MHD flow which includes the significance over a semi-infinite inclined permeable plate. A magnetic field of uniform intensity B_0 is provided in the y-direction, which is usual to the flow direction, with the x-axis measured along the plate. External flow has a constant velocity U_∞ and occurs in a direction parallel to the slanted plate. The plate is maintained at a constant temperature T_w whereas the ambient temperature T_∞ where $T_w > T_\infty$. The plate and ambient species concentrations as C_w and C_∞ are considered. Figure 1 shows the flow diagram of the modal. The effects of MHD, radiation, Joule heating, porous media, and slips condition are all being examined. Thermophoresis is considered to get a precise look at the mass deposit on the plate's surface. The following governing equations describe continuity, momentum, or energy as flows:[30–32].

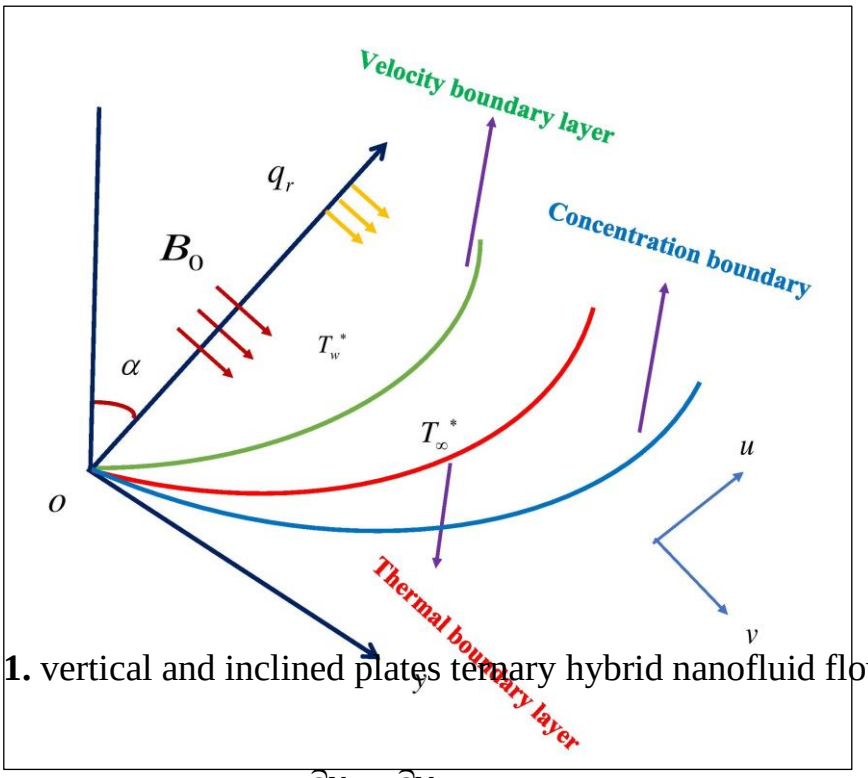

Figure 1. vertical and inclined plates ternary hybrid nanofluid flows

$$\frac{\partial u}{\partial x} + \frac{\partial v}{\partial y} \tag{1}$$

$$\rho_f\left(u\frac{\partial u}{\partial x}+v\frac{\partial u}{\partial y}\right)=\mu_f\frac{\partial^2 u}{\partial y^2}+\cos\alpha\left[g\left(\rho\beta_1\right)_f\left(T-T_\infty\right)+g\left(\rho\beta_2\right)_f\left(T-T_\infty\right)^2\right] + c\cos\alpha\left[g\left(\rho\beta_1^*\right)_f\left(C-C_\infty\right)+g\left(\rho\beta_2^*\right)_f\left(C-C_\infty\right)^2\right]-\sigma_f B_0{}^2u-\mu_f\frac{u}{k_1} \tag{2}$$

$$u\frac{\partial T}{\partial x}+v\frac{\partial T}{\partial y}=\frac{k_f}{(\rho c_p)_f}\left(\frac{\partial^2 T}{\partial y^2}\right)-\frac{1}{(\rho c_p)_f}\frac{\partial q_r}{\partial y}+\frac{\mu_f}{(\rho c_p)_f}\left(\frac{\partial u}{\partial y}\right)^2+\frac{\sigma_f}{(\rho c_p)_f}B_0{}^2u^2 \tag{3}$$

$$u\frac{\partial C}{\partial x}+v\frac{\partial C}{\partial y}=D\left(\frac{\partial^2 C}{\partial y^2}\right)-\frac{\partial V_T C}{\partial y} \tag{4}$$

Boundary conditions

$$\left.\begin{array}{lll} v=\pm v_w(x),\ \ u=U_0+L_2\dfrac{\partial u}{\partial y}\ ,\quad T=T_w+L_1\dfrac{\partial T}{\partial y},\ \ C=C_w+L_3\dfrac{\partial C}{\partial y}=0 & as & y\ \to 0 \\ u=0,\qquad T=T_\infty,\qquad C=C_\infty & as & y\ \to \infty. \end{array}\right\} \tag{5}$$

The following similarity transmutations are taken into consideration:

$$\eta=y\sqrt{\frac{U_0}{2\nu x}},\ \theta(\eta)=\frac{T-T_\infty}{T_w-T_\infty},\psi=\sqrt{2\nu x U_0}\,f(\eta),\ \phi(\eta)=\frac{C-C_\infty}{C_w-C_\infty} \tag{6}$$

Steam functions are as flows

$$u=\frac{\partial \psi}{\partial y}\ \text{and}\ \ v=-\frac{\partial \psi}{\partial x} \tag{7}$$

$$u=U_0 f^{'}(\eta)\ \text{and}\ v=-\sqrt{\frac{\nu U_0}{2x}}\left(f-\eta f^{'}\right) \tag{8}$$

Substituting Equations (6) and (8) into Equations (2) – (5) gives

$$f'''+ff''+\gamma\cos\alpha\left(\theta+\delta_1\theta^2+N(\phi+\delta_1\phi^2)\right)-K\ f'-M\ f'=0 \tag{9}$$

$$(1+Rd)\theta''+\Pr f\theta'+\Pr Ec\ f''^2+\Pr EcM\left(f'\right)^2=0 \tag{10}$$

$$\phi''+Scf\phi'-Sc\tau\theta'\phi'-Sc\tau\phi\theta''=0 \tag{11}$$

Boundary condition

$$\left.\begin{array}{l} f'(0)=1+D_1 f''(0),\quad f(0)=S,\quad \theta(0)=1+D_2\,\theta'(0),\qquad \phi(0)=1+D_2\,\phi'(0) \\ f'(\infty)=0,\qquad \theta(\infty)=0,\qquad \phi(\infty)=0. \end{array}\right\} \tag{12}$$

Here the radiation heat flux q_r , With higher orders disregarded, T^4 represents the temperature as a linear Taylor series T function. $T^4\cong 4T_\infty^{\ 3}T-3T_\infty^{\ 4}$

It can be done to determine the thermophoretic velocity V_T via surface mass fluxing.

$$V_T=\frac{\partial T}{\partial y}=-k\nu\frac{\nabla T}{T_r} \tag{13}$$

One expression for the thermophoretic coefficient k is

$$k = \frac{2C_s\left(\frac{\lambda_g}{\lambda_p} + C_t K_n\right)\left[\left(1+K_n\right)\left(C_1 + C_2 e^{-C_3/K_n}\right)\right]}{\left[\left(1+3C_m K_n\right)\left(1+2\frac{\lambda_g}{\lambda_p} + 2C_t K_n\right)\right]} \tag{14}$$

Here C_1, C_2, C_3, C_m *and* C_s are the constants.

The thermophoretic coefficient, denoted by *k*, may take on values between $(0.2 \le k \le 1.2)$.

We may express the thermophoretic parameter as

$$\tau = -\frac{k\left(T_w - T_\infty\right)}{T_r} \tag{15}$$

These parameters may be analytically defined as follows:

$$\begin{aligned} &q_r = \frac{-4\sigma^*}{3k^*}\frac{\partial T^4}{\partial y},\ M = \frac{\sigma_f {B_0}^2 2x}{U_0 \rho_f},\ Rd = \frac{4\sigma^* {T_\infty}^3}{3\,k_f k^*},\ \mathrm{Pr} = \frac{\mu c_p}{k},\ \delta_1 = \frac{g\beta_2\left(T_w - T_\infty\right)}{\beta_1}, \\ &\delta_2 = \frac{g{\beta_2}^*\left(C_w - C_\infty\right)}{\beta_1^*},\ \mathrm{Re}_x = \frac{U_0 2x}{\nu},\ K = \frac{2x\nu}{U_0 k_1},\ Ec = \frac{{U_0}^2}{c_p\left(T_w - T_\infty\right)},\ \gamma = \frac{Gr_x}{\mathrm{Re}_x}, \\ &Gr_x = \frac{g\beta_1\left(T_w - T_\infty\right)\left(2x\right)^3}{\nu^2},\ S = -v_w\sqrt{\frac{2x}{\nu U_0}},\ Sc = \frac{\nu}{D}, \end{aligned} \tag{16}$$

3. Engineering quantities

3.1. A measure of skin friction coefficient

It is written in the following manner: $Cf_x = \frac{\tau_w}{\rho(U_0)^2}$. The following is a definition of shear stress:

$$\tau_w = \mu_f\left(\frac{\partial u}{\partial y}\right)_{y=0} \tag{17}$$

Finally, we have

$$Cf_x\,\mathrm{Re}_x^{-1/2} = 2f''(0) \tag{18}$$

3.2. Nusselt number

The essential physical quantities are the heat transfer, which is expressed as

$$Nu_x = \frac{xq_w}{k_f\left(T_w - T_\infty\right)} \tag{19}$$

Where q_w is the surface heat flow in the x-direction, which is determined.

$$q_w = -\left(k_f + \frac{16\sigma T_\infty^{\ 3}}{3k^*} \right)\left[\frac{\partial T}{\partial y} \right]_{y=0}$$

we have

$$Nu_x \, \mathrm{Re}_x^{-1/2} = -(1+Rd)\,\theta'(0) \tag{20}$$

3.3. Sherwood number

The essential physical quantities are the rate of Sherwood no, which is expressed as

$$Sh = \frac{J_s}{U_0 C_\infty} \tag{21}$$

Where J_s is the surface mass fluxing perceived as

$$J_s = -D\left(\frac{\partial C}{\partial y} \right)_{y=0}$$ than

we have

$$Sh_x \, \mathrm{Re}_x^{1/2} = -\phi'(0) \tag{22}$$

4. Numerical Approach

The governing equations are transformed into an initial value issue by letting $f(\eta) = g_1,\ f'(\eta) = g_2,\ f''(\eta) = g_3,\ f'''(\eta) = g_3',\ \theta(\eta) = g_4,\ \theta'(\eta) = g_5,\ \theta''(\eta) = g_5',\ \phi(\eta) = g_6,$ $\phi'(\eta) = g_7,\ \phi''(\eta) = g_7'.$ then there are reduced to

$$f''' = -\left(ff'' + \gamma \cos\alpha \left(\theta + \delta_1\theta^2 + N(\phi + \delta_1\phi^2) \right) - K\ f' - M\ f' \right) \tag{23}$$

$$\theta'' = -\frac{\left(\mathrm{Pr}\ f\theta' + \mathrm{Pr}\, Ec\,(f'')^2 + \mathrm{Pr}\, EcM\,(f')^2 \right)}{(1+Rd)} \tag{24}$$

$$\phi'' = -\left(Scf\phi' - Sc\tau\theta'\phi' - Sc\tau\phi\theta'' \right) \tag{25}$$

boundary conditions are

$$\left.\begin{array}{l} f(0) = S, \quad f'(0) = 1 + D_1 f''(0), \quad \theta(0) = 1 + D_2\,\theta'(0), \quad \phi(0) = 1 + D_2\,\phi'(0) \\ f'(\infty) = 0, \quad \theta(\infty) = 0, \quad \phi(\infty) = 0. \end{array}\right\} \tag{26}$$

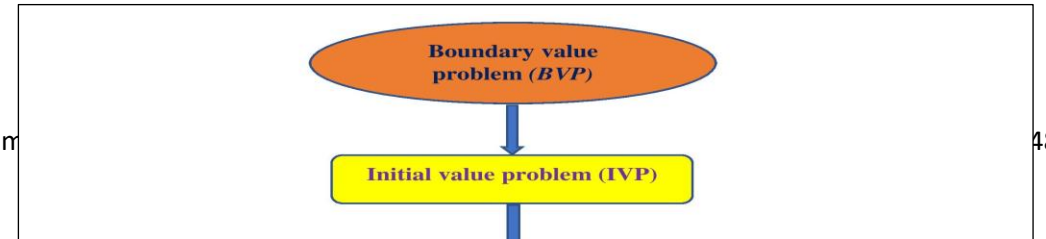

The equations (23)-(26) can be expressed as

Figure 5. RK-4 Method flow chart

$$\begin{bmatrix} g_1' \\ g_2' \\ g_3' \\ g_4' \\ g_5' \\ g_6' \\ g_7' \end{bmatrix} = \begin{bmatrix} g_2 \\ g_3 \\ -\left(g_1 g_3 + \gamma \cos\alpha \left(g_4 + \delta_1 g_4^{\,2} + N(g_6 + \delta_1 g_6^{\,2})\right) - K\ g_2 - M\ g_2\right) \\ g_5 \\ -\dfrac{\left(\Pr g_1 g_5 + \Pr Ec\left(g_3\right)^2 + \Pr EcM\left(g_2\right)^2\right)}{\left(1+Rd\right)} \\ y_5 \\ -\left(Scg_1 g_7 - Sc\tau g_5 g_7 - Sc\tau g_6 g_7'\right) \end{bmatrix} \tag{27}$$

Boundary condition is

$$\left.\begin{array}{ll} g_1 = S, \quad g_2 = 1 + D_1 g_3, g_4 = 1 + D_2 g_4, \ y_6 = 1 + D_3 g_7, & at\ \ \eta = 0 \\ y_2 = 0, \quad y_4 = 0\ , y_6 = 0 & at\ \ \eta = \infty \end{array}\right\} \tag{28}$$

In these above Equation 27 uses the MAPLE software and R-K^{4th} order with the shooting method Ref in Figure 5. As a result, the leading equations are solved in equations (28), lengthwise with their boundary's. Limiting asymptotic conditions in Equation (28) $\eta \to \infty$ was revived by an imperfect set of efforts η , says η a state when there is no discernible difference in temperature, velocity, concentration profile, and all effects parameters. This performance is generally regarded

as satisfactory in the domain of boundary layer analysis. When attempting to solve an issue, step scope with $\Delta\eta = 0.01$. It's better to be realistic about the inward converging condition 10^{-6} under all circumstances.

6. Confirmation of Results

This study of the heat transfer and mass transfer thermal radiation and mixed convection slip flow over a porous inclined plate with thermophoresis. The governing nonlinear duo Partial Differential Equations are translated into ordinary differential equations via similarity transmutations and then solved through the Maple software solver by using the Numerical Method (RK-4th Order). Dimensionless parameters values are constant in the following $Rd = 0.1$, $\gamma = 1$, $N = 0.5$, $\tau = 1$, $K = 0.5$, $D_1 = 0.3, D_2 = 0.3, D_3 = 0.3$, $M = 1.0$, $\delta_1 = 2, \delta_2 = 0.4$, $Pr = 0.7$, $Ec = 0.1$, $S = 0.5$, $Sc = 0.5$, $\alpha = 90^\circ$ is the vertical plate and $\alpha = 30^\circ$ is the inclined plate is considered. The influence of active variables, including the magnetic parameter (*M*), ($S > 0$) suction, ($S < 0$) injection, porosity (*K*), α angle of inclination, buoyancy force (γ), thermal radiation (*Rd*), (*Pr)* Prandtl number, (*N)* is the buoyancy ratio parameter, (δ_1) is nonlinear temperature parameter,(δ_2) nonlinear concentration parameter, *Sc* is Schmidt number, (τ) thermophoresis parameter, (*Ec*) Eckert number on discussed velocity profiles $f'(\eta)$, Temperature profiles $\theta(\eta)$, concentration profiles $\phi(\eta)$, skin-friction, Nusselt number, and Sherwood number. These parameters are represented through graphs.

6.1 *Velocity profile*

Figures 2-7 show the effects of the magnetic field (*M*), porosity (*K*), and buoyancy force (γ), α angles vertical plate, (δ_1) is nonlinear temperature parameter,(δ_2) nonlinear concentration parameter on velocity $f'(\eta)$ for inclined vertical plates. Figure 2 demonstrations the influence of the magnetic field on the velocity $f'(\eta)$ of inclined vertical plates. As the magnetic field strength rises, the $f'(\eta)$ decreases across inclined vertical plates. The magnetic force and Lorentz force it produces together are known as the resistive force because they cause velocity to decrease in the physical universe. Figure 3 shows the consequence of porosity (*K*) on the velocity $f'(\eta)$ across an inclined plate. As the porosity medium (*K*) increases, the velocity decreases across inclined plates. As the porosity variable (*K*) rises, so does the friction force between nanoparticles. Figure 4 demonstrates the result of buoyancy force (γ) on the velocity $f'(\eta)$ over an inclined plate. As the buoyancy increases, the velocity profile rises across inclined plates. Figure 5 illustrates the consequence of angle (α) on the velocity $f'(\eta)$ of inclined plates. As the γ increases, the velocity profile decreases through inclined plates. Figure 6 proves the result of is nonlinear temperature parameter (δ_1) on the velocity $f'(\eta)$ over an inclined plate. As the δ_1 increases, the velocity profile rises across inclined plates. Figure 7 demonstrates the result of nonlinear concentration (δ_2) on the velocity $f'(\eta)$ over an inclined plate. As the δ_2 increases, the velocity profile rises across inclined plates. Figure 5 illustrates the consequence of angle (α) on the velocity $f'(\eta)$ of inclined plates. As the γ increases, the velocity profile decreases through inclined plates.

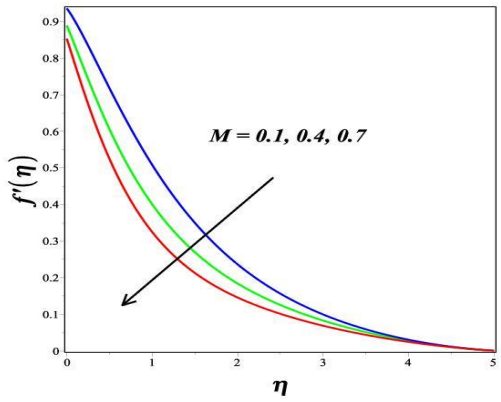

Figure 2. The consequence of M on the $f'(\eta)$

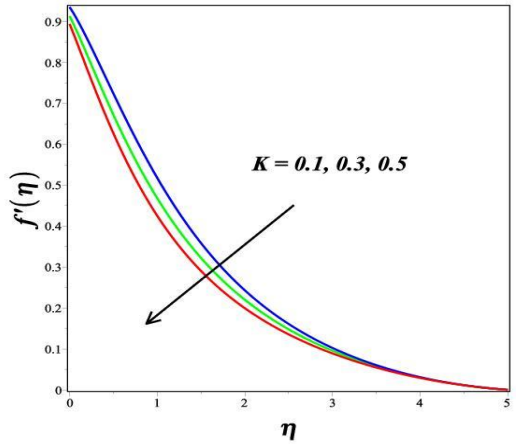

Figure 3. The consequence of K on the $f'(\eta)$

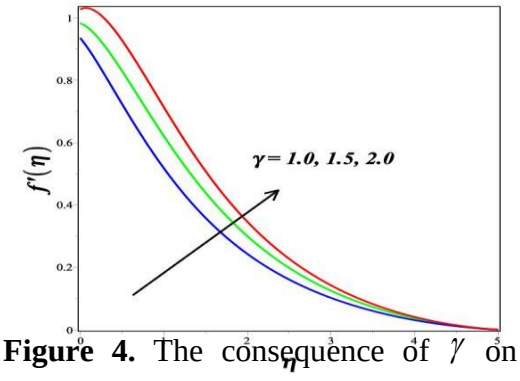

Figure 4. The consequence of γ on the $f'(\eta)$

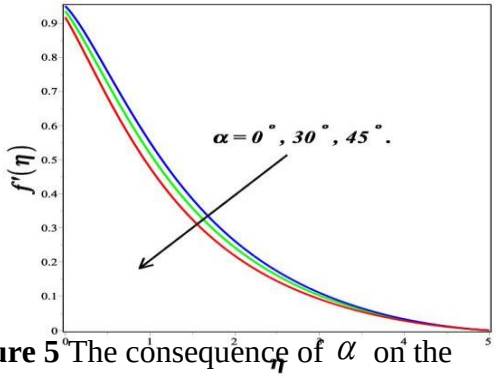

Figure 5 The consequence of α on the $f'(\eta)$.

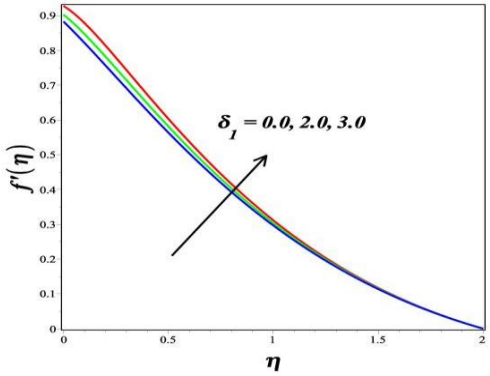

Figure 6. The consequence of δ_1 on the $f'(\eta)$

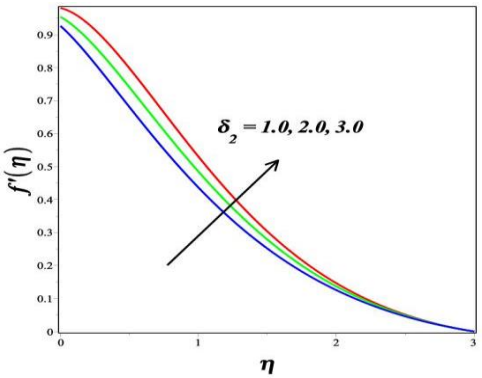

Figure 7 The consequence of δ_2 on the $f'(\eta)$

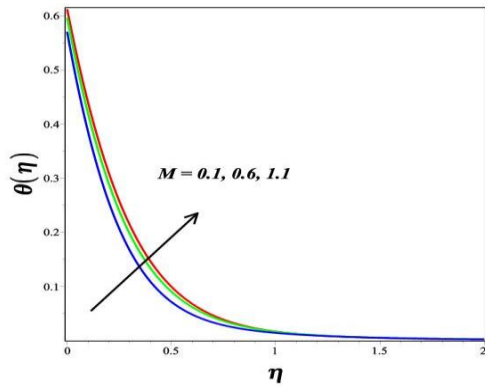

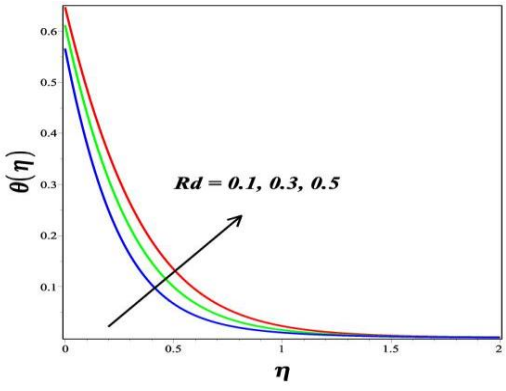

Figure 8. The consequence of M on the $\theta(\eta)$.

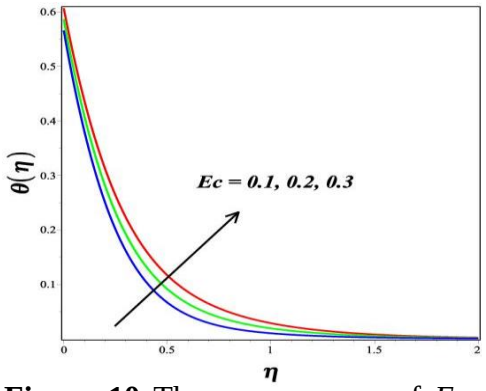

Figure 10 The consequence of Ec on the $\theta(\eta)$.

Figure 9. The consequence of Rd on the $\theta(\eta)$.

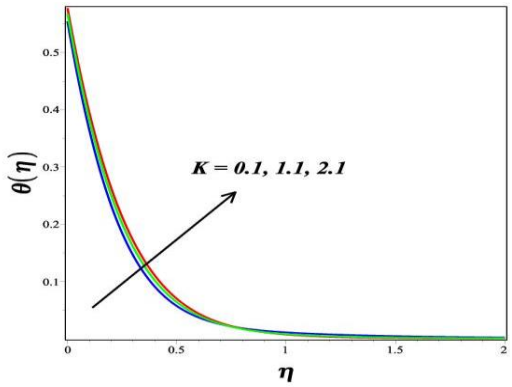

Figure 11 The consequence of K on the $\theta(\eta)$.

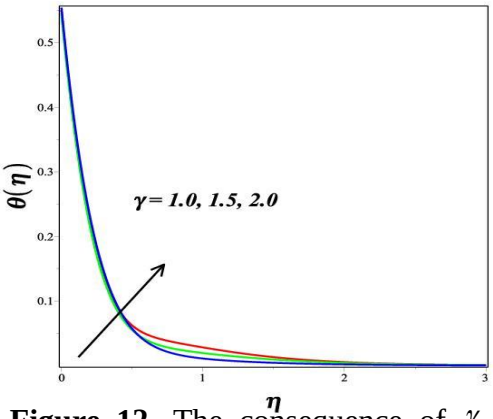

Figure 12. The consequence of γ on the $\theta(\eta)$.

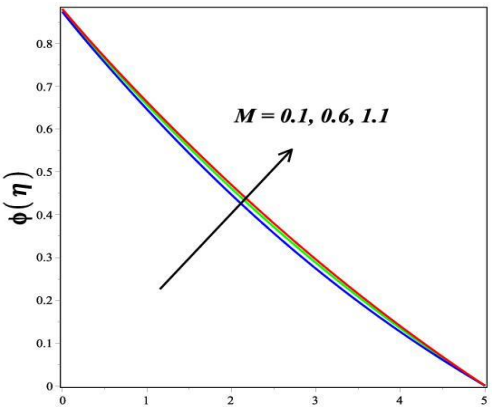

Figure 13. The consequence of M on the $\phi(\eta)$.

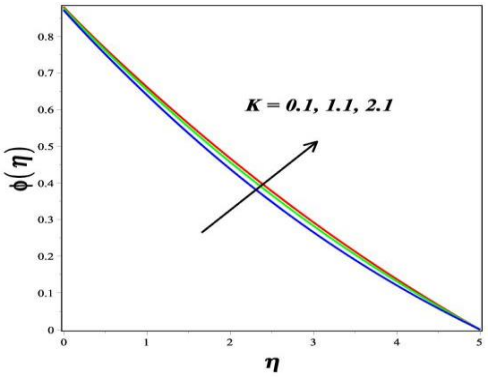

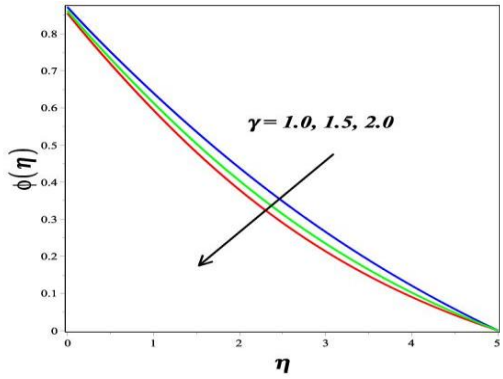

Figure 14. The consequence of K on the $\phi(\eta)$

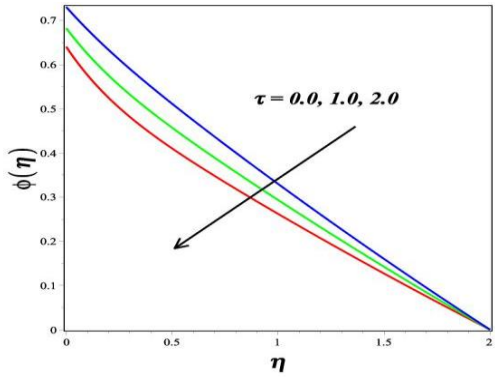

Figure 16. The consequence of τ on the $\phi(\eta)$.

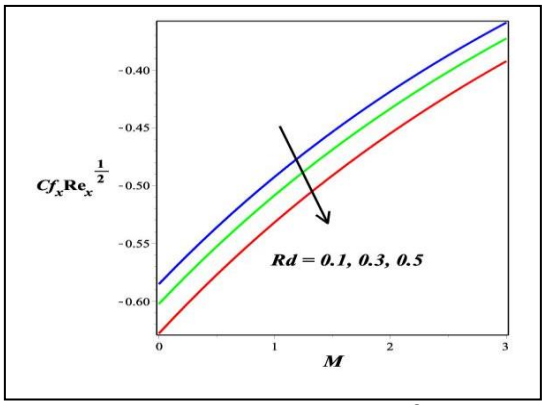

Figure 18. The consequence of *Rd* and *M* on the $Cf_x \operatorname{Re}_x^{1/2}$

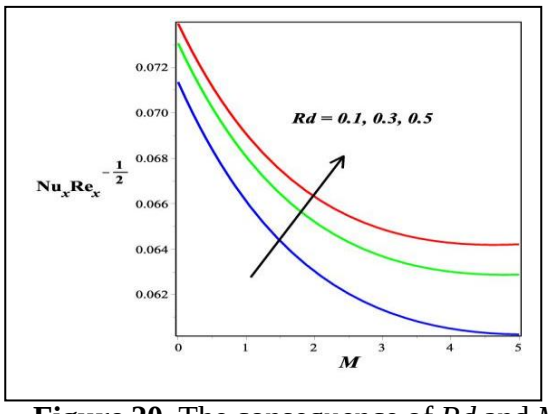

Figure 20. The consequence of *Rd* and *M* on the $Nu_x \operatorname{Re}_x^{-1/2}$

Figure 15. The consequence of γ on the $\phi(\eta)$

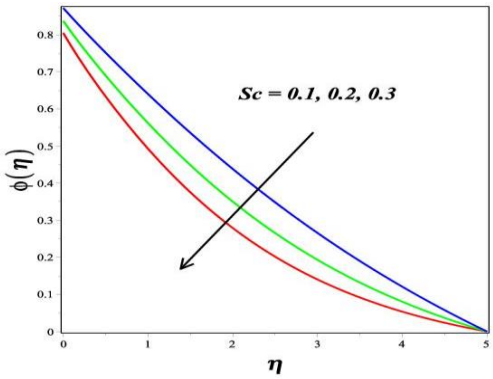

Figure 17. The consequence of Sc on the $\phi(\eta)$.

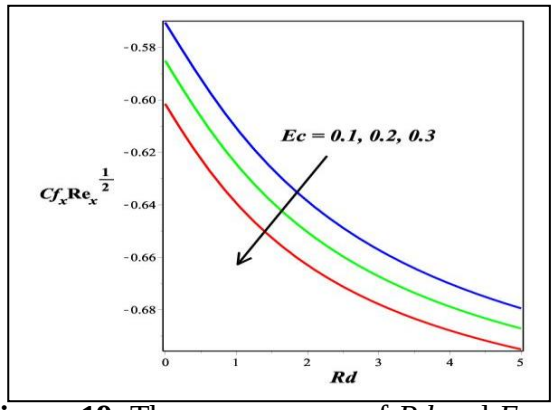

Figure 19. The consequence of *Rd* and *Ec* on the $Cf_x \operatorname{Re}_x^{1/2}$

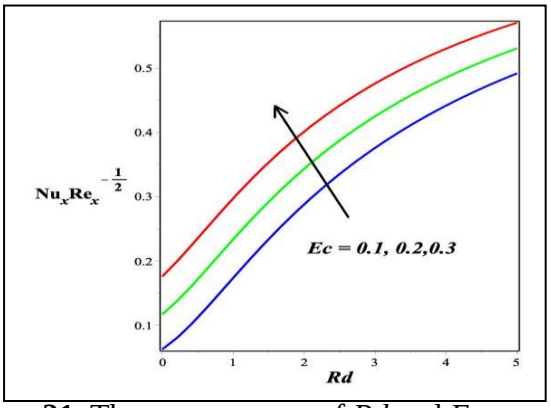

Figure 21. The consequence of *Rd* and *Ec* on the $Nu_x \operatorname{Re}_x^{-1/2}$

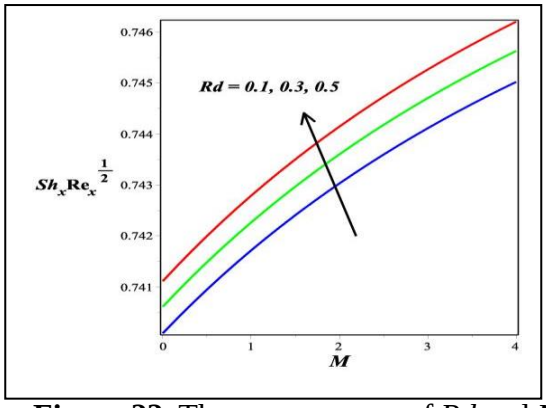

Figure 22. The consequence of *Rd* and *M* on the $Sh_x \mathrm{Re}_x^{1/2}$

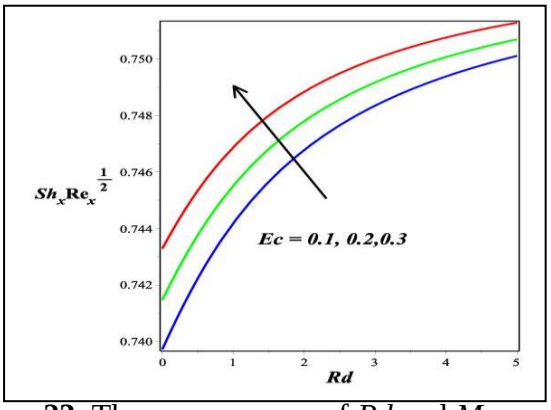

Figure 23. The consequence of *Rd* and *M* on the $Sh_x \mathrm{Re}_x^{1/2}$

Figure 6 proves the result of is nonlinear temperature parameter (δ_1) on the velocity $f'(\eta)$ over an inclined plate. As the δ_1 increases, the velocity profile rises across inclined plates. Figure 7 demonstrates the result of nonlinear concentration (δ_2) on the velocity $f'(\eta)$ over an inclined plate. As the δ_2 increases, the velocity profile rises across inclined plates.

6.2 *Temperature profiles*

In Figures 8-12, the inclined plates on the Temperature profile $\theta(\eta)$ are shown for several influence parameters such as *M*, *Rd*, *Ec*, *K*, and γ. Figures 8 demonstrate the consequences of the *M* on the temperature $\theta(\eta)$ over inclined plates. As the magnetic field strength grows, it also increases the temperature across the inclined plates. Due to the Lorentz force. Figure 9 illustrates the impression of *Rd* on temperature $\theta(\eta)$ over an inclined plate. As the thermal radiation rises, the temperature profile increases through inclined plates. Physically, the fact that the thermal radiation flux rises as the flow progresses the $\theta(\eta)$ so enhances the flow development. Figure 10 shows the inspiration of the Eckert number on the temperature profile $\theta(\eta)$ over inclined plates. As the *Ec* rises, the $\theta(\eta)$ increases through inclined plates. Figure 11 shows the consequence of porosity (*K*) on the temperature profile across an inclined plate. As the porosity medium (*K*) increases, the temperature increases across inclined plates. Figure 12 shows the result of buoyancy force (γ) on the temperature profile $\theta(\eta)$ over an inclined plate. As the buoyancy increases, the $\theta(\eta)$ profile increases across inclined plates

6.2 Concentration profiles

Figures 13-17 show the consequence of the magnetic field (*M*), porosity (*K*), and buoyancy force (γ), *Sc* which is the Schmidt number, τ thermophoresis parameter on concentration profiles $\phi(\eta)$ for inclined vertical plates. Figure 13 demonstrations the consequences of the *M* on the $\phi(\eta)$ over inclined plates. As the magnetic field strength grows, it also increases the concentration across the inclined plates. Since the fluid contains electricity, the magnetic field produces an opposite force recognized as the Lorentz force, which slows down the flow of the fluid. Because of this impact,

the fluid heats up, speeding up the concentration of species in the free stream and improving concentration profiles. Figure 14 displays the consequence of porosity (K) on the concentration profiles $\phi(\eta)$ across an inclined plate. As the porosity medium (K) increases, the $\phi(\eta)$ increase across inclined plates. Figure 15 shows the result of buoyancy force (γ) on the concentration profiles $\phi(\eta)$ over an inclined plate. As the buoyancy increases, the $\phi(\eta)$ profile decreases across inclined plates. Figure 16 illustrations the outcome of τ the thermophoresis parameter on the $\phi(\eta)$ over an inclined plate. As the τ thermophoresis increases, the $\phi(\eta)$ profile decreases across inclined plates. Since the thermophoresis effect reduces the thermal boundary layer, this also means that the concentration boundary layer thickens as the rate of the effect rises. Figure 17 demonstrations the effect of Sc on the $\phi(\eta)$ over an inclined plate. As the Sc Schmidt number increases, the $\phi(\eta)$ profile decreases across inclined plates.

The impression of *Ec, Rd,* and *M* on skin friction $Cf_x \operatorname{Re}_x^{-1/2}$ over an inclined plate is seen in Figures 18 and 19. Observing the effect of the $Cf_x \operatorname{Re}_x^{-1/2}$ many values of radiation *Rd*, *Ec and* Magnetic field (*M)* is haggard. It has been observed that this $Cf_x \operatorname{Re}_x^{-1/2}$ is a decrease. The impression of *Ec*, *Rd,* and *M* on Nusselt number $Nu_x \operatorname{Re}_x^{-1/2}$ for over an inclined plate are seen in Figures 20 and 21. Observing the effect of the $Nu_x \operatorname{Re}_x^{-1/2}$ many values of radiation *Rd*, *Ec and* Magnetic field (*M)* is haggard. It has been observed that this $Nu_x \operatorname{Re}_x^{-1/2}$ is a growing function with Rd, *Ec*, and *M* increasing for inclined plates. The impression of Ec, *Rd*, and *M* on Sherwood number $Sh_x \operatorname{Re}_x^{-1/2}$ for over an inclined plate are seen in Figures 22 and 23. Observing the effect of the $Sh_x \operatorname{Re}_x^{-1/2}$ many values of radiation *Rd*, *Ec, and* Magnetic field *M* is haggard. It has been observed that this $Sh_x \operatorname{Re}_x^{-1/2}$ is a growing function with Rd, *Ec*, and *M* increasing for inclined plates.

Table. 2 2 A comparison Stanton numbers some literature such consider the values $Sc = 1000, M = Ec = \delta_1 = \delta_2 = 0$ *and* $\alpha = 90^{\circ}$.

τ	S	Mills et al. [33]	Tsai [34]	Alam et al. [35]	Jha and Samaila [30]	Present results
1	1	0.8619	0.9134	0.8691	0.8693	0.8683
1	0.5	0.5346	0.5598	0.5359	0.5368	0.5358
1	0.0	0.2095	0.2063	0.2076	0.2081	0.2071
1	-0.004	0.2068	0.2034	0.2070	0.2089	0.2085
1	-0.005	0.2062	0.2027	0.2065	0.2073	0.2071
1	-0.25	0.0344	0.0295	0.0349	0.0359	0.0352

7. Conclusions

This study employs heat transfer and mass transfer analysis of MHD buoyancy-driven mixed convection slips flow over a porous inclined plate with thermophoresis. The governing nonlinear coupled partial differential equations are converted into ordinary differential equations via similarity transformations. The NM is used in the MAPLE software to compute the graphical results of the flow parameters. The effects of temperature, velocity, concentration, heat transfer, skin friction coefficients, and Sherwood number on physical parameters like a magnetic field, porosity, buoyancy force and buoyancy ratio parameter, thermal radiation, Schmidt number, and thermophoresis are discussed through graphs. It has many applications, such as aerodynamic extrusion of plastic sheets, including die-extruded polymer sheets, glass-blowing-spun fibres, continuous casting, and biomedical uses in antimicrobial agents, diagnostic, and drug delivery. The research's most important results are discussed here,

- The velocity profile decreases over inclined plates while the porosity and magnetic field parameters increase.
- As the values of the thermal radiation, magnetic field, buoyancy-driven mixed convection, and porosity parameters increase, the temperature increases.
- As the magnetic field and porosity parameters rise, inclined plate concentration profiles increase.
- As the Schmidt number and thermophoresis parameters rise, inclined plate concentration profiles decrease.
- As skin friction across an inclined plate is reduced, the impression of Ec, Rd, and M values rises.
- The impression of *Ec*, *Rd*, and *M* values grows as the Nusselt number and Sherwood number over an inclined plate rise.

NOMENCLATURE			
A	Constant	**Greek symbols**	
B_0	Magnetic field induction	T	The temperature at the surface
D_1	Velocity slip parameter	T_W	Surface Temperature
D_2	Temperature slip parameter	T_∞	Ambient Fluid temperature
D_2	Mass slip parameter	v_w	Transpiration velocity
$Cf_x \, \mathrm{Re}_x^{-1/2}$	Coefficient of skin friction	x, y	Axis in the direction along and normal to the plate
c_p	Specific heat	ρ	Fluid density
C_1, C_2, C_3	Constants	β	Casson fluid parameter
Ec	Eckert number	μ	Fluid dynamic viscosity
Gr_x	Local Grashof number	α_1	Temperature ratio parameter
g	Acceleration due to gravity	α_2	concentration ratio parameter
k	Thermal conductivity	β_1, β_2	Thermal expansion coefficient for temperature
K	Porosity parameter	β_1^*, β_2^*	Thermal expansion coefficient for concentration

N	Buoyancy ratio parameter	ν	Kinetic viscosity
M	Magnetic parameter	σ	Electrical conductivity
$Nu_x \, \mathrm{Re}_x^{-1/2}$	Nusselt number	θ	The dimensionless Temperature of a fluid
Pr	Prandtl number	ψ	Steam function
q_r	Radiative heat flux	τ_w	Wall shear stress
q_w	Surface heat flux	η	Similarity variable
Re_x	Local Reynolds number	σ^*	Stefan-Boltzmann constant
Rd	Thermal Radiation parameter	γ	Local buoyancy parameter
S	Suction / Injection parameter	λ_1	Heat generation parameter
Sc	Schmidt number	k^*	Mean absorption coefficient

References:

1. I. A. Badruddin, Z. A. Zainal, P. A. A. Narayana, K. N. Seetharamu, and L. W. Siew, Int. J. Numer. Methods Eng. **65**, 2265 (2006).

2. U. Khan, A. Zaib, S. Abu Bakar, and A. Ishak, Case Stud. Therm. Eng. **26**, 101150 (2021).

3. M. G. Reddy, M. V. V. N. L. Sudharani, and K. G. Kumar, Contin. Mech. Thermodyn. **32**, 971 (2020).

4. D. V. K. Prasad, G. S. K. Chaitanya, and R. S. Raju, Results Eng. **3**, 100019 (2019).

5. S. Bilal, K. K. Asogwa, H. Alotaibi, M. Y. Malik, and I. Khan, Alexandria Eng. J. **60**, 4243 (2021).

6. X. Qiang, I. Siddique, K. Sadiq, and N. A. Shah, Alexandria Eng. J. **59**, 4171 (2020).

7. K. Raghunath, J. Nanofluids **12**, 767 (2023).

8. P. Sudarsana Reddy, A. J. Chamkha, and A. Al-Mudhaf, Adv. Powder Technol. **28**, 1008 (2017).

9. M. Goyal and R. Bhargava, Int. J. Appl. Comput. Math. **4**, 1 (2018).

10. M. Mustafa, Int. J. Heat Mass Transf. **108**, 1910 (2017).

11. A. Rauf, N. Ali Shah, A. Mushtaq, and T. Botmart, AIMS Math. **8**, 164 (2023).

12. N. Abbas, W. Shatanawi, and T. A. M. shatnawi, Alexandria Eng. J. **70**, 179 (2023).

13. K. Ahmed, T. Akbar, I. Ahmed, T. Muhammad, and M. Amjad, Numer. Heat Transf. Part A Appl. **0**, 1 (2023).

14. K. Sakkaravarthi and P. B. A. Reddy, Proc. Inst. Mech. Eng. Part E J. Process Mech. Eng. 1 (2022).

15. M. Qayyum, T. Abbas, S. Afzal, S. T. Saeed, A. Akgül, M. Inc, K. H. Mahmoud, and A. S. Alsubaie, Coatings **12**, (2022).

16. M. Y. Ali, S. Reza-E-Rabbi, M. M. H. Rasel, and S. F. Ahmmed, Partial Differ. Equations Appl. Math. **7**, 100500 (2023).

17. U. Khan, A. Zaib, and A. Ishak, Mathematics **9**, 921 (2021).

18. B. Ali, A. Shafiq, I. Siddique, Q. Al-Mdallal, and F. Jarad, Case Stud. Therm. Eng. **28**, 101537 (2021).

19. N. Gulle and R. Kodi, Mater. Today Proc. **50**, 2218 (2021).

20. P. Maghsoudi, G. Shahriari, H. Rasam, and S. Sadeghi, J. Cent. South Univ. **26**, 1294 (2019).

21. Y. M. Chu, F. Alzahrani, O. Mopuri, C. Ganteda, M. I. Khan, P. Jaya Lakshmi, S. U. Khan, and S. M. Eldin, Case Stud. Therm. Eng. **42**, 102695 (2023).

22. B. Ahmad, M. Ozair Ahmad, M. Farman, A. Akgül, and M. B. Riaz, South African J. Chem. Eng. **43**, 135 (2023).

23. B. V. Swarnalathamma, D. M. P. Babu, and M. V. Krishna, J. Comput. Math. Data Sci. **5**, 100069 (2022).

24. R. N. Barik and G. C. Dash, Appl. Math. Comput. **226**, 423 (2014).

25. K. Sakkaravarthi and P. B. A. Reddy, Proc. Inst. Mech. Eng. Part C J. Mech. Eng. Sci. (2022).

26. A. Nayan, N. I. F. A. Fauzan, M. R. Ilias, S. F. Zakaria, and N. H. Z. Aznam, J. Adv. Res. Fluid Mech. Therm. Sci. **92**, 51 (2022).

27. D. Sarma and K. K. Pandit, Ain Shams Eng. J. **9**, 631 (2018).

28. G. Revathi, J. B. Macherla, C. S. Raju, R. Sharma, and A. J. Chamkha, J. Nanofluids **10**, 75 (2021).

29. S. Mukhopadhyay and G. C. Layek, Int. J. Heat Mass Transf. **51**, 2167 (2008).

30. B. K. Jha and G. Samaila, Numer. Heat Transf. Part B Fundam. **83**, 139 (2023).

31. A. Selim, M. A. Hossain, and D. A. S. Rees, Int. J. Therm. Sci. **42**, 973 (2003).

32. M. S. Alam, M. M. Rahman, and M. A. Sattar, Int. J. Therm. Sci. **47**, 758 (2008).

33. A. F. Mills, H. Xu, and F. Ayazi, Int. J. Heat Mass Transf. **27**, 1110 (1984).

34. R. Tsai, Int. Commun. Heat Mass Transf. **26**, 249 (1999).

35. M. S. Alam, M. M. Rahman, and M. A. Sattar, Commun. Nonlinear Sci. Numer. Simul. **14**, 2132 (2009).